Phase Behavior of the [N(CH)][BF]-[N(CH)][BF] Binary System

AUTHOR(S):

WANG, Yushen; NONAKA, Ryojun; MATSUMOTO, Kazuhiko; HAGIWARA, Rika

CITATION:

WANG, Yushen ...[et al]. Phase Behavior of the [N(CH)][BF]-[N(CH)][BF] Binary System. Electrochemistry 2018, 86(2): 52-56

ISSUE DATE:

2018-03-05

URL:

http://hdl.handle.net/2433/245221

Phase behavior of the $[N(C_2H_5)_4][BF_4]$-$[N(C_3H_7)_4][BF_4]$ binary system

Yushen Wang, Ryojun Nonaka, Kazuhiko Matsumoto, Rika Hagiwara*

Graduate School of Energy Science, Kyoto University, Yoshida, Sakyo-ku, Kyoto 606–8501, Japan

Phone: +81 75 753 5822, Fax: +81 75 753 5906,

E–mail: k-matsumoto@energy.kyoto-u.ac.jp (Kazuhiko Matsumoto)

Abstract

Phase behavior of the $[N_{2222}][BF_4]$-$[N_{3333}][BF_4]$ (N_{2222}^+ = tetraethylammonium, and N_{3333}^+= tetrapropylammonium,) binary system has been investigated by differential scanning calorimetry and powder X-ray diffraction. Two solid-solid phase transitions are observed in differential scanning calorimetric curve in the range of $x([N_{3333}][BF_4])$ = 0.1-0.9 ($x([N_{3333}][BF_4])$ = the molar fraction of $[N_{3333}][BF_4]$) reflecting the solid-solid phase transition of each single salt, and only slight shift was observed for the transition temperatures. Powder X-ray diffraction patterns confirmed phase transitions. Although the amount of the minor constituent is low in the solid solution phase based on each single salt at 313, 373 K, and 423 K, Phase I of $[N_{2222}][BF_4]$ at 483 K with the NaCl-type structure, which is regarded as an ionic plastic crystal (IPC) phase, can accommodate $[N_{3333}][BF_4]$ up to the level where significant change in lattice parameter is observed (5.7 % volume expansion). Drop of the liquidus line was observed for the salts with the mixing ratio $x([N_{3333}][BF_4])$ = 0.8 to 0.9 approaching to the eutectic temperature of 475 K. Ionic conductivity of Phase I increases by two orders of magnitude from $x([N_{3333}][BF_4])$ = 0 to 0.1 owing to the lattice expansion by inclusion of N_{3333}^+.

.

1. Introduction

Ionic plastic crystals (IPCs), which are composed of only cations and anions, have recently been studied as a new class of ion conductors due to their liquid-like degrees of freedom, negligible vapor pressure, as well as specific structures including globular or flexible frame, or lattice defects such as vacancies, that lead to good mobility of target ions and increase ionic conductivity.[1-11] In particular, organic ionic plastic crystals (OIPCs) are attractive for the application as solid-state electrolytes because of the greater structural flexibility than simple inorganic salts.[8,12] Because of the similarity in chemical structures of ionic species used in IPC and ionic liquid materials, chemistry of OIPCs is often regarded as an extended field of ionic liquids. The plastic crystal phase is commonly reached via a solid-solid phase transition with increasing temperature and is often associated with an order-disorder transition.[4] Ionic plastic crystals are composed of highly disordered component ions, and have disordered structures which can result in a small entropy change of melting (ΔS_m).[13,14] Owing to the disorder originating from rotational motions of the ions, it is often difficult to precisely determine the structure of OIPCs.[3,12,15-17]

During considerable efforts to increase the ionic conductivity of OIPCs, the method of doping of the salts of target ions into OIPCs has been adopted since it was reported to significantly increase the ionic conductivity up to several orders of magnitude.[5,7,9,18-23] Among these materials, [*N*-ethyl-*N*-methylpyrrolidinium][$N(SO_2CF_3)_2$] was one of the OIPCs to exhibit high ionic conductivity, and doping with Li[$N(SO_2CF_3)_2$] salt to this OIPC was found to result in enhancement in ionic conductivity by twenty times and was very attractive for lithium secondary battery application.[5,19,20] Addition of an inorganic salt to OIPCs has been mainly carried out to introduce mobile ions such as Li^+ to achieve good ion conduction, whereas mixing two OIPCs is also considered as a method to obtain high ionic conductivity, which typically focuses on the change of their structural and thermal properties.[24]

Alkylammonium salts have been attracting attention in structural studies because they exhibit a variety of structural changes during thermal transitions and their highest temperature solid phase is often characterized as IPC phase.[25-27] Our previous study on plastic crystal phases of tetraalkylammonium salts of BF_4^- and PF_6^- showed that the size of the ions affects the structural type of their plastic crystal phases,

which follows the radius ratio rule.[28] The NaCl-type structure was confirmed by indexing powder X-ray diffraction patterns for the plastic crystal phase of some salts with small cations such as N_{2222}^+ (tetraethylammonium, see Figure 1). Other structural types such as the CsCl-type were also identified in the plastic crystal phase for tetraalkylammonium salts. Simplification of structure with high symmetry upon phase transition is one of the unique characteristics of plastic crystals.[29]

So far, few studies have been done to elucidate the formation of solid solutions between tetraalkylammonium salts, in particular for plastic crystal phases. In our recent study, the formation of solid solution in the plastic crystal phase of the $[N_{2222}][BF_4]$-$[N_{2222}][PF_6]$ binary system was confirmed by combination of several analytical methods.[24] In this anion-mixing system, both the crystal and plastic crystal phases form solid solutions, along with the decreased transition temperature from the crystal phase to plastic crystal phase compared to single salts. The NaCl-type solid solution was identified in this plastic crystal phase at any ratio, and the *a* lattice parameter increased linearly with increasing $[N_{2222}][PF_6]$ ratio, which followed the Vegard's law.[30] Although ionic conductivity was not high enough in this binary system, it provides a good model to study the formation of solid solutions in binary alkylammonium salts.

In the present study, thermal and structural behavior of the $[N_{2222}][BF_4]$-$[N_{3333}][BF_4]$ binary system (see Figure 1 for the chemical structures of N_{2222}^+, N_{3333}^+, and BF_4^-) is reported, where effects of cation mixing on formation of solid solutions is mainly investigated. Phase transition and structure at each fraction of $[N_{3333}][BF_4]$ are investigated by differential scanning calorimetry (DSC) and powder X-ray diffraction (XRD) measurements.

2. Experimental

2.1 Chemicals. All non-volatile materials were handled in a glove box under an atmosphere of dry Ar. All volatile materials were handled in a vacuum line made of stainless steel and PFA (tetrafluoroethylene-perfluoroalkylvinylether copolymer). The tetrafluoroborate salts, $[N_{2222}][BF_4]$ (Aldrich, purity 98%) and $[N_{3333}][BF_4]$ (Aldrich, purity 98%) were purchased and dried under vacuum at 353 K for 24 h. All the mixed samples with $x([N_{3333}][BF_4])$ = 0.1-0.9 were pelletized into a disk (10 mm in diameter and *ca.* 1

mm in thickness) and heat-treated at 473 K under vacuum for 24 h to ensure the mutual diffusion of ionic species. After the heat treatment, the samples were kept at room temperature for at least three weeks to ensure that the phase of each sample is stable at room temperature.

2.2 Analysis. Differential scanning calorimetric curve was obtained by a DSC-8230 Thermo Plus EVO II Series (Rigaku Corp.) at a scan rate of 5 K min^{-1}. The samples for DSC were sealed in an airtight Al cell under an atmosphere of dry Ar. Enthalpy change of each transition was obtained based on the heat flow in the DSC curve, and the entropy change was calculated by dividing the enthalpy change by the transition temperature. Each transition temperature was determined using the tangent intersection method. Powder XRD was recorded by a SmartLab X-ray diffractometer (Rigaku Corp.) equipped with a D/teX Ultra 250 silicon strip detector and graphite-monochromated Cu-Kα radiation (1.5418 Å; 40 kV-30 mA). The well-ground sample was spread on a sample holder (Cr-Cu alloy) and placed in a temperature controlling apparatus. The measurement was performed under vacuum at a scanning rate of 1 K min^{-1}. The obtained data was indexed by DICVOL06.[31] Ionic conductivity was measured under an Ar atmosphere by an AC impedance technique using an impedance analyzer 3532-80 (Hioki E.E. Corp.).The samples were pelletized into a disk (10 mm diameter and *ca.* 1 mm thickness) and were placed between two stainless steel disk electrodes, fixed in a alumina tube. The cell was sandwiched between two stainless steel plates with two glass sheets insulating the cell from the holder.

3. Results and discussion

3.1 Thermal properties. Figure 2 shows DSC curves for the first heating scan of the $[N_{2222}][BF_4]$-$[N_{3333}][BF_4]$ binary system and Table 1 lists the corresponding DSC data. According to our previous study of the $[N_{2222}][BF_4]$-$[N_{2222}][PF_6]$ binary system, the successive cooling and the second heating scans were not reproducible due to the slow kinetics for the phase transition during cooling process.[24] It also occurred in the $[N_{2222}][BF_4]$-$[N_{3333}][BF_4]$ binary system, and the data during the first heating scan was used for further discussion. The $[N_{2222}][BF_4]$ and $[N_{3333}][BF_4]$ single salts exhibit one solid-solid transition at 343 K and 395 K (the onset temperature of transition), respectively, corresponding to crystal-plastic crystal

phase transition. Three endothermic peaks are also observed in the range of $x([N_{3333}][BF_4])$ = 0.1−0.9. Microscopic observation confirmed the peak around 475 K is due to the appearance of the liquid phase and a two-phase region occurs above this transition temperature. Complete liquid phase appears around 500 K in the case of $x([N_{3333}][BF_4])$ = 0.8 and 0.9, whereas liquid phase was not confirmed in the present temperature range of $x([N_{3333}][BF_4])$ = 0−0.7. According to X-ray diffraction analysis below, the two transitions around 345 and 400 K are assigned to solid-solid phase transitions. The solid-solid transition temperatures in the range of $x([N_{3333}][BF_4])$ = 0.1−0.9 slightly decrease compared to the ones of the pure compounds, which results from the formation of solid solutions (see the section of XRD for details). Although a small but detectable endothermic peak, which could be due to a minor structural change, is observed around 410 K, this was not reproducible and omitted from the following discussion. The enthalpy and entropy changes of the solid-solid transitions around 345 K tend to decrease as $x([N_{3333}][BF_4])$ increases, whereas those of the solid-solid transitions around 400 K shows the opposite trend. This suggests that these transitions originate from the transition from Phase II to Phase I of each single salt.

3.2 Structures of the crystal and plastic crystal phases. According to DSC analysis, three endothermic peaks were observed in the range of $x([N_{3333}][BF_4])$ = 0.1−0.9. The structures before and after each phase transition were analyzed by powder XRD at selected temperatures of 313, 373, 423 and 483 K. Figure 3 shows the XRD patterns of the $[N_{2222}][BF_4]$-$[N_{3333}][BF_4]$ binary system ($x([N_{3333}][BF_4])$ = 0−1.0) at 313 K and 373 K. Diffraction peaks belonging to Phase II of both $[N_{2222}][BF_4]$ and $[N_{3333}][BF_4]$ are observed at 313 K in the range of $x([N_{3333}][BF_4])$ = 0.1−0.9 (Figure 3(a)), and peak intensity changes according to the change of $x([N_{3333}][BF_4])$. Slight peak shift is observed between $x([N_{3333}][BF_4])$ = 1.0 and 0.9, suggesting formation of solid solution. In accordance with the previous work,[24] the $[N_{2222}][BF_4]$ single salt transforms to Phase I with the NaCl-type structure (Figure 3(b)). The diffraction patterns at 373 K in the range of $x([N_{3333}][BF_4])$ = 0.1−0.9 are composed of the diffraction peaks assigned to Phase I of $[N_{2222}][BF_4]$ and Phase II of $[N_{3333}][BF_4]$ by reflecting the behavior of the single salts. The degree of peak shift is still not significant at this temperature, either. It should be noted that, neat $[N_{2222}][BF_4]$ shows a

plastic crystal phase at 373 K. Thus the combination of $[N_{2222}][BF_4]$ with $[N_{3333}][BF_4]$ does not extend the range of the plastic crystal phase to lower temperature side, which agrees with the DSC analysis.

Figure 4(a) shows the XRD patterns of the $[N_{2222}][BF_4]$-$[N_{3333}][BF_4]$ binary system ($x([N_{3333}][BF_4])$ = 0-1.0) at 423 K. The diffraction peaks assigned to Phase I of $[N_{2222}][BF_4]$ and $[N_{3333}][BF_4]$ appeared at this temperature, because the $[N_{3333}][BF_4]$ single salt transforms at 395 K to Phase I with the $TBPPF_6$-type ($TBPPF_6$ = tetrabutylphosphoniumhexafluorophosphate)[28] structure. The peak shift is also very small in both the phases.

Figure 4(b) shows the XRD patterns of the $[N_{2222}][BF_4]$-$[N_{3333}][BF_4]$ binary system ($x([N_{3333}][BF_4])$ = 0-1.0) at 483 K. The single salts have the lattice parameters of a = 10.883(9) Å for $[N_{2222}][BF_4]$ and a = 14.250(7) Å for $[N_{3333}][BF_4]$ at this temperature. In the range of $x([N_{3333}][BF_4])$ = 0.1−0.8, only the diffraction peaks assigned to Phase I of $[N_{2222}][BF_4]$ were observed, whereas at $x([N_{3333}][BF_4]) = 0.9$, only the diffraction peaks assigned to Phase I of $[N_{3333}][BF_4]$ were observed. This observation indicates that liquid phase appears at this temperature by mixing the two salts. Compared to the slight peak shift observed between $x([N_{3333}][BF_4])$ = 0.9 and 1.0, the diffraction peaks significantly shift between $x([N_{3333}][BF_4])$ = 0 and 0.1. This suggests that lattice expansion of the NaCl-type structure based on the $[N_{2222}][BF_4]$single salt by doping of $[N_{3333}][BF_4]$ is more significant than lattice contraction of the $TBPPF_6$-type structure based on the $[N_{3333}][BF_4]$ single salt by doping of $[N_{2222}][BF_4]$. The amount of $[N_{3333}][BF_4]$ is considered to be below 10 mol% since the diffraction peak position is almost identical above $x([N_{3333}][BF_4]) \geq 0.1$ and the diffraction peaks assigned to $[N_{3333}][BF_4]$ are not observed at $x([N_{3333}][BF_4])$ = 0.1. The a lattice parameter of the NaCl-type cubic cell estimated from the data at $x([N_{3333}][BF_4]) = 0.1$ is 11.087(4) Å, indicating the 5.7 % lattice expansion from the original $[N_{2222}][BF_4]$ single salt. This is in contrast to the contraction of the $TBPPF_6$-type cubic cell from $x([N_{3333}][BF_4])$ = 1.0 to 0.9 (a = 14.189(2) Å at $x([N_{3333}][BF_4]) = 0.9$, volume contraction = 1.3 %).

In a previous work, radii of ions in OIPCs were estimated by the hard sphere model.[28] In this procedure, the radius of PF_6^- was first calculated from disordered inorganic salts,[32,33] and those of organic cations and BF_4^- were calculated from the lattice parameters of OIPCs, assuming the ions behave as hard sphere.

The resulting radii of N_{2222}^+, N_{3333}^+, BF_4^-, and PF_6^- are 3.34, 3.71, 2.07, and 2.37 Å, respectively. The cation-mixing $[N_{2222}][BF_4]$-$[N_{3333}][BF_4]$ system in this study gives solid solution in only limited ranges near $x([N_{3333}][BF_4]) = 0$ and 1.0, whereas the anion-mixing $[N_{2222}][BF_4]$-$[N_{2222}][PF_6]$ system forms solid solution with the NaCl-type structure at any mixing ratio. This difference suggests that the substitution of the smaller constituent ion (anion in this case) in solid solution is easier than that of the larger constituent ion (cation in this case). This may be explained by the close packing model, because the cation is considered to be closely packed (or close to that) compared to the anion in these salts and has more effect on the volume of crystal lattice. For example, volume change from $x([N_{3333}][BF_4]) = 0$ to 0.1 for the $[N_{2222}][BF_4]$-$[N_{3333}][BF_4]$ system is 5.7 % and is significantly larger than 0.82 % from $x([N_{2222}][PF_6]) = 0$ to 0.1 for the $[N_{2222}][BF_4]$-$[N_{2222}][PF_6]$ system.

3.3 Phase diagram and ionic conductivity. The phase diagram of the $[N_{2222}][BF_4]$-$[N_{3333}][BF_4]$ binary system based on the DSC and XRD results is shown in Figure 5. The two-phase region of solid $[N_{2222}][BF_4]$ and $[N_{3333}][BF_4]$ in their respective phases (denoted as I and II) appears. Meanwhile, there are two narrow regions of solid solutions in both the sides of the phase diagram. These two solid solution phases are denoted as $[N_{2222}][BF_4]$ss and $[N_{3333}][BF_4]$ss. The crystal to plastic crystal transition temperature only slightly decreases upon mixing, which differs from the $[N_{2222}][BF_4]$-$[N_{2222}][PF_6]$ binary system.[24] The eutectic point is found between $x([N_{3333}][BF_4]) = 0.8$ and 0.9. Therefore, above the highest transition temperature, the IPC($[N_{2222}][BF_4]$ss)+Liquid two-phase region appears between $x([N_{3333}][BF_4]) = 0.1$ and 0.8, and the IPC($[N_{3333}][BF_4]$ss)+Liquid two-phase region appears between $x([N_{3333}][BF_4]) = 0.8$ and 0.9, which is much narrower than the former.

The difficulty in the formation of a solid solution in the plastic crystal phase results from the different structures of the $[N_{2222}][BF_4]$ and $[N_{3333}][BF_4]$ single salts, as well as the different sizes of N_{2222}^+ and N_{3333}^+. In the $[N_{2222}][BF_4]$-$[N_{2222}][PF_6]$ binary system, solid solutions forms via random substitution of PF_6^- or BF_4^-. However, in the $[N_{2222}][BF_4]$-$[N_{3333}][BF_4]$ binary system, sizes of N_{2222}^+ and N_{3333}^+ are quite different, causing the substitution difficulty.

Ionic conductivity of the $[N_{2222}][BF_4]$ single salt in the plastic crystal phase was quite low (2.4×10^{-6} mS cm^{-1} at 423 K) due to the low mobilities of component large ions. Although the impact is not spectacular as in the case of addition of Li salts,[5] addition of 10 mol% $[N_{3333}][BF_4]$ improved the ionic conductivity by two orders of magnitude (3.5×10^{-4} mS cm^{-1} at 423 K). The effects of lattice expansion are considered to contribute to this behavior.

4. Conclusion

The present study reported phase behavior of the $[N_{2222}][BF_4]$-$[N_{3333}][BF_4]$ binary system. Although this system forms solid solution in an only limited range of $x([N_{3333}][BF_4])$ at low temperatures, the highest temperature solid phase with the NaCl-type structure based on the $[N_{2222}][BF_4]$ single salt can accommodate $[N_{3333}][BF_4]$ below $x([N_{3333}][BF_4]) = 0.1$. The phase diagram shows the drop of liquid line by mixing two components and slight decrease in solid-solid phase transition temperature. Ionic conductivity of the NaCl-type structure increases roughly two orders of magnitude from $x([N_{2222}][BF_4]) = 0$ to 0.1 owing to the lattice expansion by inclusion of N_{3333}^+. Substitution of the larger component ions seems to be difficult because they sustain the crystal lattice by closely packing themselves. However, even a slight amount of minor constituent ion can expand lattice enough to raise ionic conductivity.

Acknowledgements

This work was supported by Kansai Research Foundation for Technology Promotion.

REFERENCES

1. H. Han, J. Nie, K. Liu, W. Li, W. Feng, M. Armand, H. Matsumoto, Z. Zhou, Electrochim. Acta, 55 (2010) 1221-1226.
2. W. A. Henderson, V. G. Young, S. Passerini, P. C. Trulove, H. C. De Long, Chem. Mater., 18 (2006) 934-938.
3. W.A.Henderson, M. Herstedt, V.G.Young, S.Passerini, H.C.De Long, P.C.Trulove,Chem.Mater., 45 (2006) 934-938.

4. J.M. Pringle, P.C. Howlett, D.R. MacFarlane, M. Forsyth,J. Mater. Chem., 20 (2010) 2056-2062.
5. D. R. MacFarlane, J. Huang, M. Forsyth, Nature, 402 (1999) 792-794.
6. D. R. MacFarlane, P. Meakin, N. Amini, M. Forsyth, J. Phys.: Condens. Matter, 13 (2001) 8257–8267.
7. Y. Zhou, X. Wang, H. Zhu, M. Armand, M. Forsyth, G.W. Greene, J.M. Pringle, P.C. Howlett, Phys. Chem. Chem. Phys., 19 (2017) 2225-2234.
8. J.M. Pringle, Phys. Chem. Chem. Phys., 15 (2013) 1339-1351.
9. D. R. MacFarlane, M. Forsyth, Adv. Mater., 13 (2001) 957-966.
10. M. Moriya, T. Watanabe, W. Sakamoto, T. Yogo, RSC Advances, 2 (2012) 8502-8507.
11. Z. Zhou, H. Matsumoto, Electrochem. Commun., 9 (2007) 1017-1022.
12. L. Jin, K.M. Nairn, C.M. Forsyth, A.J. Seeber, D.R. MacFarlane, P.C. Howlett, M. Forsyth, J.M. Pringle, J. Am. Chem. Soc., 134 (2012) 9688-9697.
13. S.Forsyth, J.Golding, D.R.MacFarlane, M.Forsyth, Electrochim. Acta, 46 (2001) 1753-1757.
14. J. Golding, N.Hamid, D. R. MacFarlane, M. Forsyth, C. Forsyth, C. Collins, J. Huang, Chem.Mater., 13 (2001) 558-564.
15. M. Herstedt, W.A. Henderson, M. Smirnov, L. Ducasse, L. Servant, D. Talaga, J.C. Lassègues, J. Mol. Struct., 783 (2006) 145-156.
16. H. Ono, R. Ikeda, Ber. Bunsen-Ges., 100 (1996) 1833–1838.
17. H. Ishida, Y. Frukawa, S. Kashino, S. Sato, R. Ikeda, Ber. Bunsen-Ges., 100 (1996) 433–439.
18. M. Forsyth, T. Chimdi, A. Seeber, D. Gunzelmann, P.C. Howlett, J. Mater. Chem. A, 2 (2014) 3993-4003.
19. J. Huang, M.Forsyth,D.R.MacFarlane, Solid State Ionics, 136-137 (2000) 447–452.
20. M.Forsyth,J. Huang, D.R.MacFarlane, J. Mater. Chem., 10 (2000) 2259-2265.
21.S. Long, D.R.MacFarlane, M. Forsyth, Solid State Ionics, 161 (2003) 105-112.
22. Y. Shekibi, T. Ruther, J. Huang, A.F. Hollenkamp, Phys. Chem. Chem. Phys., 14 (2012) 4597-4604.
23. L. Jin, P. Howlett, J. Efthimiadis, M. Kar, D. Macfarlane, M. Forsyth, J. Mater. Chem, 21 (2011) 10171-10178.
24. K. Matsumoto, R. Nonaka, Y. Wang, G. Veryasov, R. Hagiwara, Phys. Chem. Chem. Phys., 19 (2017) 2053-2059.
25. T. Tanabe, D. Nakamura, R. Ikeda, J. Chem. Soc. Faraday Trans., 87 (1991) 987-990.
26. S. Iwai, M. Hattori, D. Nakamura, R. Ikeda, J. Chem. Soc., Faraday Trans., 89 (1993) 827-831.
27. K. Kuchitsu, H. Ono, S. Ishimaru, R. Ikeda, H. Ishida, Phys. Chem. Chem. Phys., 2 (2000) 3883-3885.
28. K. Matsumoto, U. Harinaga, R. Tanaka, A. Koyama, R. Hagiwara, K. Tsunashima, Phys. Chem. Chem. Phys., 16 (2014) 23616-23626.
29. W.J.Dunning, J. Phys. Chem. Solids, 18 (1961) 21-27.
30. A.R. Denton, N.W. Ashcroft, Physical Review A, 43 (1991) 3161-3164.
31. A. Boultif, D. Louer, J. Appl. Crystallogr., 37 (2004) 724-731.
32. K. Kitashita, R.Hagiwara, Y. Ito, O. Tamada, J. Fluorine Chem., 101 (2000) 173-179.
33. Z. Mazej, R. Hagiwara, J. Fluorine Chem., 128 (2007) 423-437.

Table 1 Summary of the DSC analysis of the $[N_{2222}][BF_4]$-$[N_{3333}][BF_4]$ binary system[a].

$x([N_{3333}][BF_4])$	T_{s1}/K	ΔH/kJ mol^{-1}	ΔS/J K^{-1} mol^{-1}
0.0	343	6.4	19

0.1	342	4.3	13
0.2	342	4.7	14
0.3	342	4.3	13
0.4	342	3.3	10
0.5	343	2.8	8.1
0.6	341	2.4	7.1
0.7	342	1.7	4.9
0.8	342	1.0	2.9
0.9	342	0.40	1.2
1.0	n.d.	--	--

$x([N_{3333}][BF_4])$	T_{s2}/K	ΔH/kJ mol^{-1}	ΔS/J K^{-1} mol^{-1}
0.0	n.d.	--	--
0.1	393	0.38	0.96
0.2	393	1.3	3.3
0.3	394	2.3	5.8
0.4	393	2.8	7.2
0.5	395	3.6	9.2
0.6	393	5.0	13
0.7	393	6.0	15
0.8	393	6.5	17
0.9	393	8.4	21
1.0	395	9.0	23

$x([N_{3333}][BF_4])$	T_{m_o}/K	T_{m_e}/K	ΔH/kJ mol^{-1}	ΔS/J K^{-1} mol^{-1}
0.0	n.d.	n.d.	--	--
0.1	n.d.	475	0.56	1.2
0.2	n.d.	475	2.0	4.1
0.3	n.d.	476	3.4	7.2
0.4	n.d.	476	4.3	9.1
0.5	n.d.	476	6.0	13
0.6	n.d.	476	7.5	16
0.7	n.d.	476	8.7	18
0.8	476	486	8.3	17
0.9	476	493	8.7	18
1.0	n.d.	514	8.0	16

[a] T_{s1} and T_{s2} denote the transition temperatures of the solid-solid transition around 345 K and 395 K, respectively. $T_{m_o}$and T_{m_e} denote the onset and final temperatures of melting process. n.d.: not detected.

Figure captions

Figure 1 Chemical structures of N_{2222}^+, N_{3333}^+, and BF_4^-.

Figure 2 Differential scanning calorimetric curves of the $[N_{2222}][BF_4]$-$[N_{3333}][BF_4]$ binary system

(x([N_{3333}][BF_4]) = 0−1.0). Scan rate: 5 K min^{-1}. Atmosphere: dry Ar.

Figure 3 X-ray diffraction patterns of the [N_{2222}][BF_4]-[N_{3333}][BF_4] binary system (x([N_{3333}][BF_4]) = 0−1.0) at (a) 313 K, and (b) 373 K. Peaks at 16.36°, 23.21°, 27.27°, and 28.52° at x[N_{3333}][BF_4] = 0 in (b) are indexed as 200, 220, 311, and 222 for the cubic cell.

Figure 4 X-ray diffraction patterns of the [N_{2222}][BF_4]-[N_{3333}][BF_4] binary system (x([N_{3333}][BF_4]) = 0−1.0) at (a) 423 K, and (b) 483 K. Peaks at 16.39°, 23.20°, 27.30°, and 28.54° at x[N_{3333}][BF_4] = 0 in (a) and at 16.34°, 23.16°, 27.21°, and 28.46° at x[N_{3333}][BF_4] = 0 in (b) are indexed as 200, 220, 311, and 222 for the cubic cell.

Figure 5 Phase diagram of the [N_{2222}][BF_4]-[N_{3333}][BF_4] binary system based on the results of DSC and XRD analysis. The symbol, ss, in the diagram denotes the solid solution. The Roman numerals in parentheses represent the solid phases of [N_{2222}][BF_4] and [N_{3333}][BF_4].

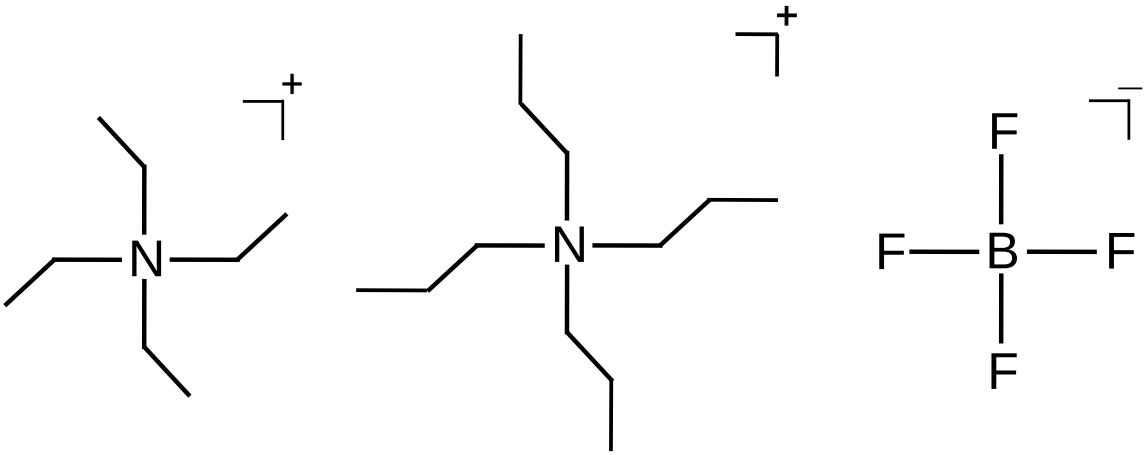

Figure 1 Chemical structures of N_{2222}^{+}, N_{3333}^{+}, and BF_4^{-}.

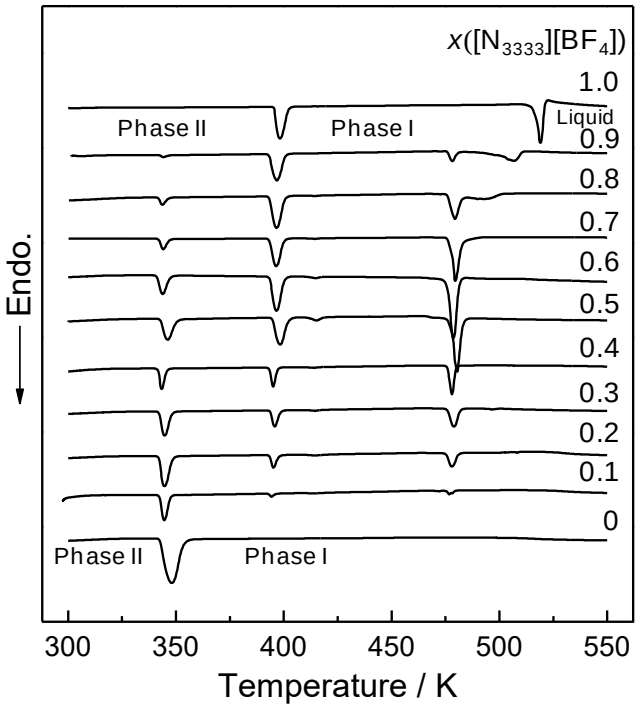

Figure 2 Differential scanning calorimetric curves of the $[N_{2222}][BF_4]$-$[N_{3333}][BF_4]$ binary system ($x([N_{3333}][BF_4])$ = 0−1.0). Scan rate: 5 K min^{-1}. Atmosphere: dry Ar.

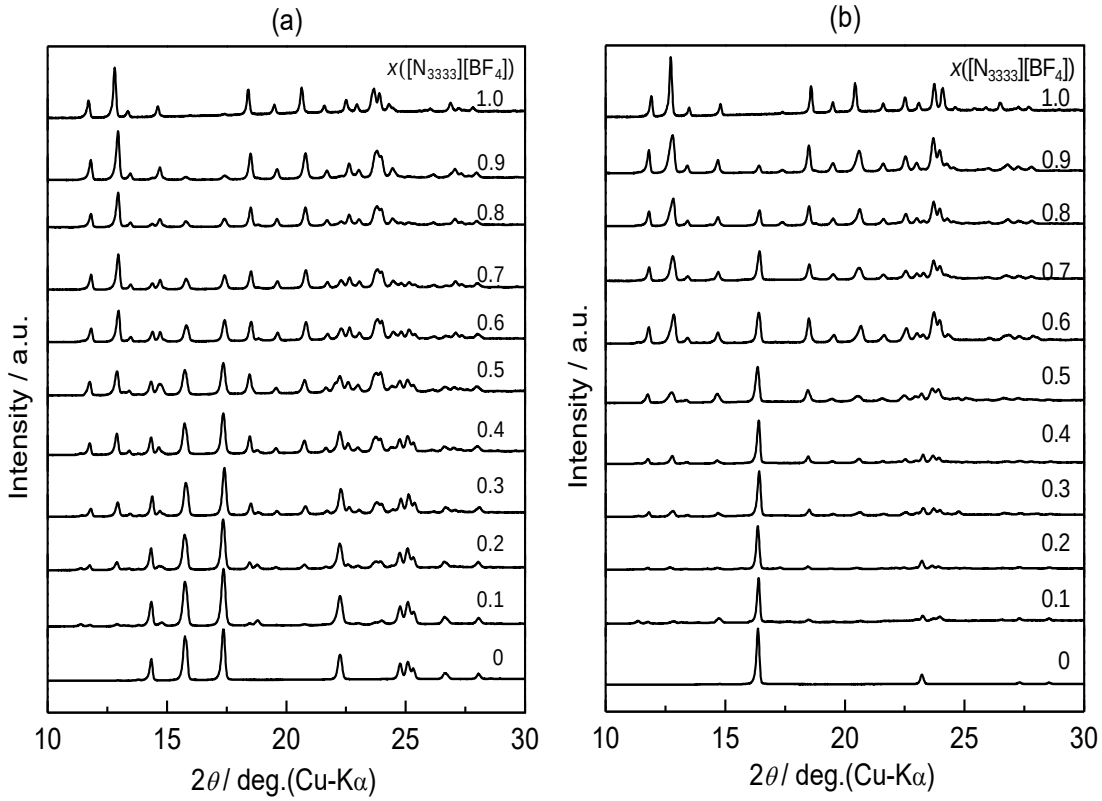

Figure 3 X-ray diffraction patterns of the $[N_{2222}][BF_4]$-$[N_{3333}][BF_4]$ binary system ($x([N_{3333}][BF_4])$ = 0−1.0) at (a) 313 K, and (b) 373 K. Peaks at 16.36°, 23.21°, 27.27°, and 28.52° at x$[N_{3333}][BF_4]$ = 0 in (b) are indexed as 200, 220, 311, and 222 for the cubic cell.

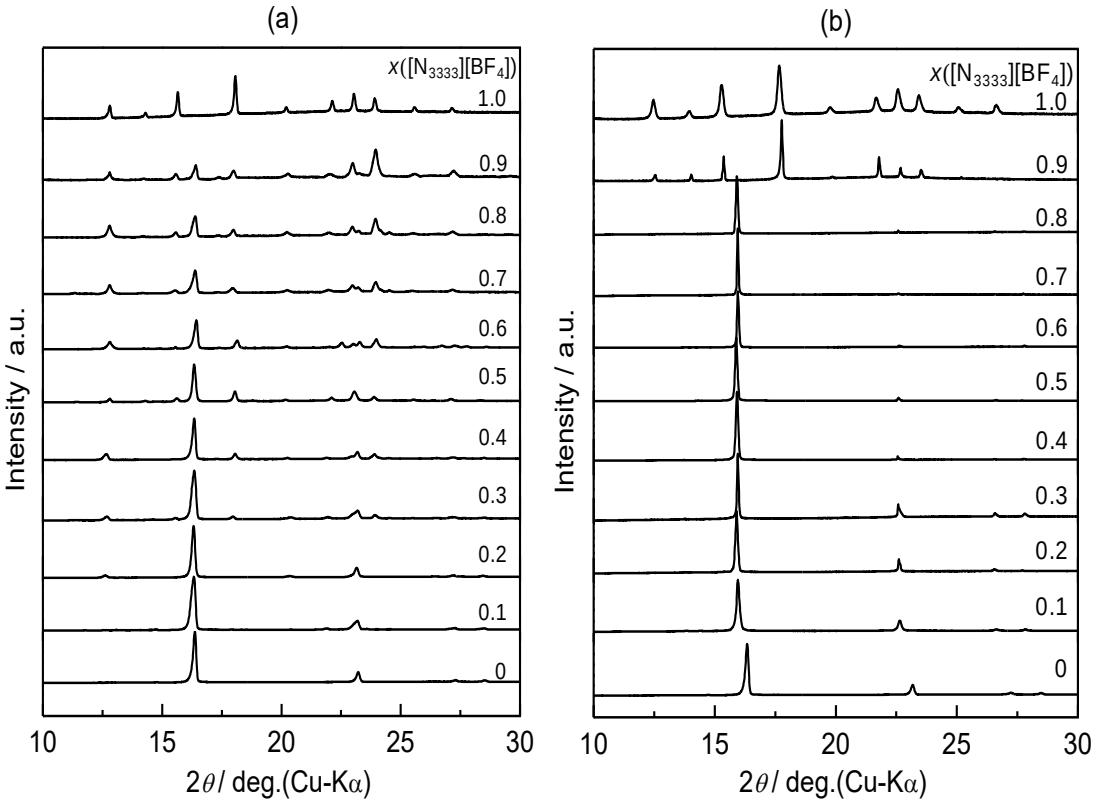

Figure 4 X-ray diffraction patterns of the $[N_{2222}][BF_4]$-$[N_{3333}][BF_4]$ binary system ($x([N_{3333}][BF_4])$ = 0−1.0) at (a) 423 K, and (b) 483 K. Peaks at 16.39°, 23.20°, 27.30°, and 28.54° at $x[N_{3333}][BF_4]$ = 0 in (a) and at 16.34°, 23.16°, 27.21°, and 28.46° at $x[N_{3333}][BF_4]$ = 0 in (b) are indexed as 200, 220, 311, and 222 for the cubic cell.

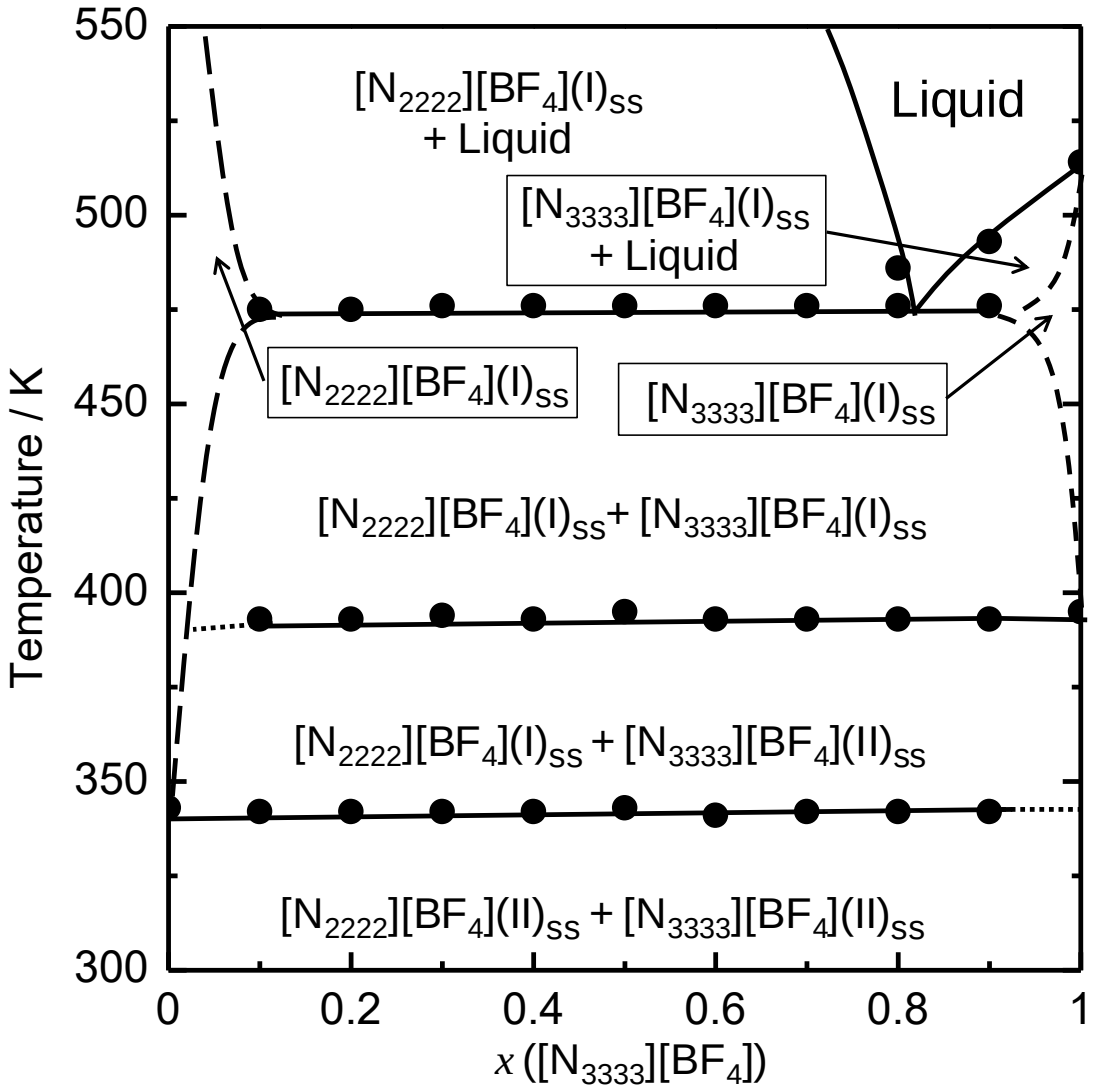

Figure 5 Phase diagram of the $[N_{2222}][BF_4]$-$[N_{3333}][BF_4]$ binary system based on the results of DSC and XRD analysis. The symbol, ss, in the diagram denotes the solid solution. The Roman numerals in parentheses represent the solid phases of $[N_{2222}][BF_4]$ and $[N_{3333}][BF_4]$.